PARALLEL MAGNETIC RESONANCE IMAGING: CHARACTERIZATION AND COMPARISON

A Thesis

by

SWATI DNYANDEO RANE

Submitted to the Office of Graduate Studies of
Texas A&M University
in partial fulfillment of the requirements for the degree of

MASTER OF SCIENCE

August 2005

Major Subject: Electrical Engineering

PARALLEL MAGNETIC RESONANCE IMAGING CHARACTERIZATION AND COMPARISON

A Thesis

by

SWATI DNYANDEO RANE

Submitted to the Office of Graduate Studies of
Texas A&M University
in partial fulfillment of the requirements for the degree of

MASTER OF SCIENCE

Approved by:

Chair of Committee,	Jim Ji
Committee Members,	Costas Georghiades
	Takis Zourntos
	James Moore
Head of Department,	Channan Singh

August 2005

Major Subject: Electrical Engineering

ABSTRACT

Parallel Magnetic Resonance Imaging:

Characterization and Comparison. (August 2005)

Swati Dnyandeo Rane, B.E., Pune University

Chair of Advisory Committee: Dr. Jim X. Ji

Magnetic Resonance Imaging (MRI) is now increasingly being used for fast imaging applications such as real-time cardiac imaging, functional brain imaging, contrast enhanced MRI, etc. Imaging speed in MRI is mainly limited by different imaging parameters selected by the pulse sequences, the subject being imaged and the RF hardware system in operation. New pulse sequences have been developed in order to decrease the imaging time by a faster k-space scan. However, they may not be fast enough to facilitate imaging in real time. Parallel MRI (pMRI), a technique initially used for improving image SNR, has emerged as an effective complementary approach to reduce image scan-time. Five methods, viz., SENSE [Pruesmann, 1999], PILS [Griswold, 2000], SMASH [Sodickson, 1997], GRAPPA [Griswold, 2002] and SPACE RIP [Kyriakos, 2000]; developed in the past decade have been studied, simulated and compared in this research. Because of the dependence of the parallel imaging methods on numerous factors such as receiver coil configuration, k-space subsampling factor, k-space coverage in the imaging environment, there is a critical need to find the method giving the best results under certain imaging conditions. The tools developed in this research help the selection of the optimal method for parallel imaging depending on a particular imaging environment and scanning parameters. Simulations on real MR phased-array data show that SENSE and GRAPPA provide better image reconstructions when compared to the remaining techniques.

ACKNOWLEDGMENTS

I would like to thank my thesis advisor Professor Jim Ji, for all the help and support he extended to me during the completion of my thesis. Special thanks to Dr. Steven Wright, Mary McDougall, Jong Bum Son and Dr. Jingfei Ma, for providing the data necessary for my experiments.

I also thank my colleagues Ravindra Garach, Yinan Liu and Yuttapong Jirarakopsakun for their timely encouragement and inspiring and enriching discussions during the group meetings.

TABLE OF CONTENTS

CHAPTER Page

LIST OF TABLES

LIST OF FIGURES

FIGURE Page

FIGURE Page

FIGURE Page

CHAPTER I

INTRODUCTION TO MAGNETIC RESONANCE IMAGING

Magnetic Resonance Imaging is a non-invasive technique to image biological tissues using the phenomenon of nuclear magnetic resonance. This phenomenon is based on the fundamental property of charged particles like protons, electrons and neutrons to posses a spin. Each individual charged particle possesses a spin or angular momentum which contributes to the MRI signal. Two or more charged particles with opposite spins tend to cancel out this signal. It is therefore, the uncancelled spins which are of importance in MRI.

A. Nuclear Magnetic Resonance

The Nuclear Magnetic Resonance phenomenon is displayed by nuclei with a net spin. Hydrogen is one such element with an unpaired (uncancelled) spin. Since hydrogen is in abundance in the human body, hydrogen protons are usually imaged to study biological tissue structure.

1. Spin Physics

Nucleus of every atom comprises of charged particles like protons. Such charged particles inside a nucleus exhibit a net spin (Fig. 1), defined by the quantum number I. Every rotating charged particle i.e. proton is associated with a magnetic moment $\vec{m}$. The magnetic moment $\vec{m}$ is related to the spin quantum number I by the following relation

$$\vec{m} = \sqrt{I \times (I+1) \times \hbar} \tag{1.1}$$

The journal model is *IEEE Transactions on Automatic Control.*

where $\hbar$ is the Planck's constant. Under equilibrium conditions, the net magnetic moment of all the protons is nullified i.e.

$$\vec{M} = \sum \vec{m} = 0 \tag{1.2}$$

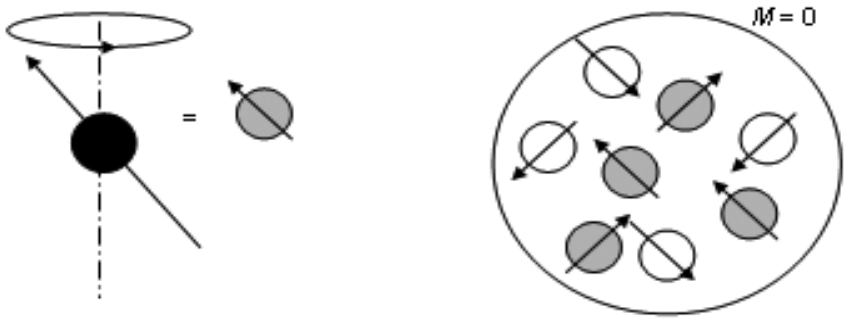

Fig. 1. Representation of proton with magnetic moment $\vec{m}$ (left). Net magnetic moment is zero (right)

When a steady magnetic field $\vec{B_0}$ is applied to these protons, the net magnetization gets aligned in the direction of $\vec{B_0}$ as shown in Fig. 2. The protons continue their precession about $\vec{B_0}$. The frequency of precession of the protons about $\vec{B_0}$ is called the *Larmor* frequency ω_0 and defined as

$$\omega_0 = \gamma B_0 \tag{1.3}$$

where γ is the gyromagnetic constant and is equal to 42.57 MHz for hydrogen. It is clear from the above equation that the *Larmor* frequency is dependent on the static field strength B_0.

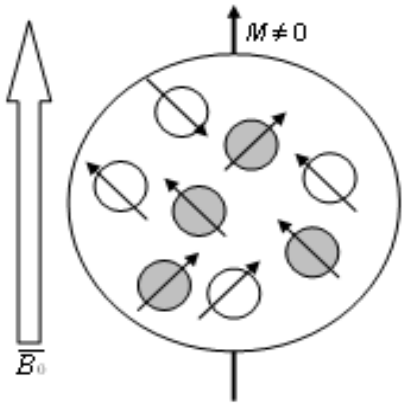

Fig. 2. Effect of steady magnetic field $\vec{B_0}$ on the protons and the net magnetization

2. Radio Frequency (RF) Field and Resonance

If the protons aligned in the direction of $\vec{B_0}$ are subject to a second RF magnetic field $\vec{B_1}$ with frequency equal to the *Larmor* frequency ω_0, the protons experience a force at resonance ($\omega = \omega_0$) which tips the net magnetization away from its equilibrium position under the effect of B_0. This field is applied only for a short duration and hence often referred to as a RF pulse. The tipping process is shown in Fig. 3.

The tipping of the net magnetization $\vec{M}$ depends on the energy of $\vec{B_1}$. For e.g., if $\vec{B_0}$ is applied along the Z direction and $\vec{B_1}$ is applied along the X axis such that $\vec{M}$ tips completely onto the X-Y plane and the z-component of $\vec{M}$, $M_z = 0$, then the $\vec{B_1}$ pulse is called the 90° pulse. This is because $\vec{M}$ is tipped away from its initial position along $\vec{B_0}$ in the z direction, by 90°. Once tipped, the protons are all in phase but they continue to precess. The protons start dephasing due to inhomogeneities in the $\vec{B_0}$ field, causing the net transverse magnetization in the X-Y plane to decrease. As soon as the $\vec{B_1}$ field is turned off, the protons relax back to equilibrium, i.e., they realign along the $\vec{B_0}$ field in the Z- direction. This change in $\vec{M_z}$ and $\vec{M_{xy}}$ components is detected by the MRI receiver to obtain the magnetic resonance signal. The MR

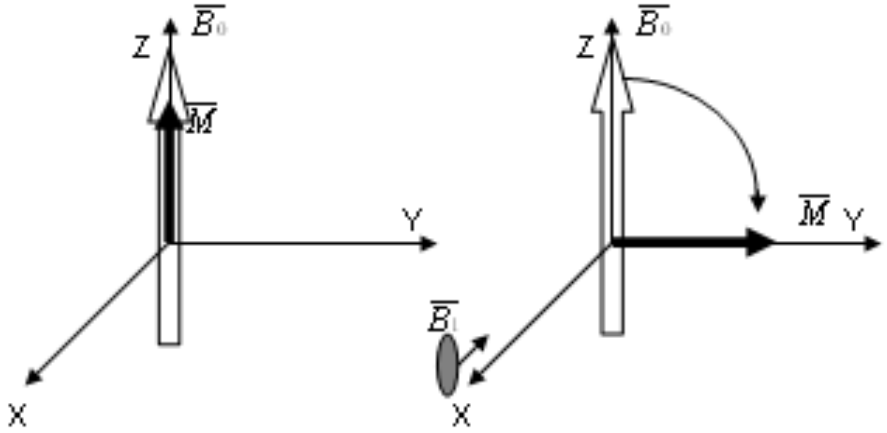

Fig. 3. The position of M before and after the application of the $\vec{B_1}$ pulse

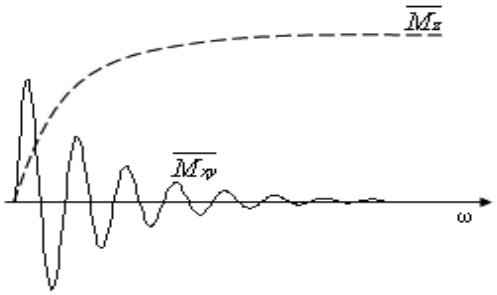

Fig. 4. Free Induction Decay

signal $\vec{M}_{xy}$ is called the Free Induction Decay (FID) and is shown in Fig. 4 .

The MR signal is characterized by the Bloch equations:

$$\frac{dM}{dt} = \gamma M \times B_0 - \frac{M_x\vec{a_x} + M_y\vec{a_y}}{T2} - \frac{M_z - M_0}{T1} \tag{1.4}$$

where T1 and T2 are the relaxation times associated with the relaxation of the longitudinal and transverse component of $\vec{M}$. $\vec{M}_x$ and $\vec{M}_y$ are the components of $\vec{M}_{xy}$ in the X and Y directions respectively. M_0 is the net magnetization at equilibrium. The Bloch equation describes the behavior of the net magnetization vector $\vec{M}$. The solu-

tion to this equation for $\vec{M}_z$ and $\vec{M}_{xy}$ signals, as shown in Fig. 4. Once the MR signal is generated, it has to be detected, stored and processed for image reconstruction.

B. Signal Localization and Imaging

Each point of the image is encoded in MRI by differentiation of the spins using a program which is known as pulse sequence. The pulse sequence determines how the magnetic fields are manipulated in order to spatially encode every location on the image. Additional fields called gradient fields are used for this purpose.

1. Gradient Fields

A gradient field is a linearly varying magnetic field. Therefore at a given point, the protons experience a net magnetic field of

$$B = B_0 + \gamma G_r \tag{1.5}$$

Thus, if a gradient field is applied along the direction of $\vec{B_0}$ (Z-direction), the *Larmor* frequency at every point along the Z-direction will be given by

$$\omega_0 = \gamma(B_0 + \gamma G_z) \tag{1.6}$$

The protons can be differentiated in the Z-direction on the basis of gradient G_z. To uniquely determine every point in an image, three gradients G_z, G_x and G_y are used to spatially encode the spins in the Z, X and Y directions respectively.

2. Slice Selection

Slices for imaging can be selected in the sagittal, coronal and axial plane of a three dimensional object using the slice selection gradient field as shown in the Fig. 5.

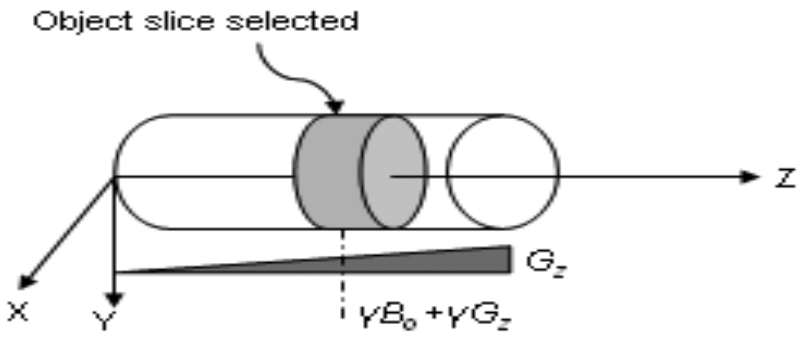

Fig. 5. Slice selection

A slice is selected using the slice selection gradient and the RF field in conjunction. Once the imaging plane is selected, every point in the image is encoded using the frequency encoding and the phase encoding gradients. The slice selection gradient is usually applied along the Z-direction.

3. Frequency Encoding

A gradient field applied along the X-direction will create a spatially varying *Larmor* frequency distribution along the X-direction. Though the gradient field is applied along the X-direction, the gradient direction is along the Z-axis as shown in Fig. 6. As a result, all points along X-direction can be encoded on the basis of the *Larmor* frequency. To encode the image data in the Y-direction, another gradient field is applied along the Y-axis.

4. Phase Encoding

Unlike the frequency encoding gradient which is turned ON for a long time to cover all data points in the X-direction, the phase encoding gradient is applied for a very short time. Using the same principle as that of frequency encoding, a frequency

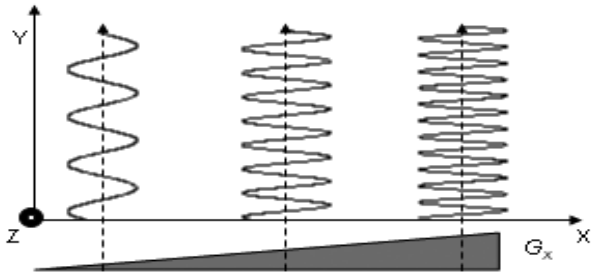

Fig. 6. Frequency difference created by the frequency encoding gradient

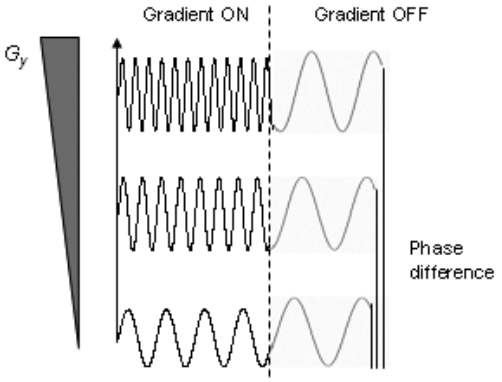

Fig. 7. Phase difference created by phase encoding gradient

difference is introduced along the Y-direction by the phase encoding gradient. Again, though the gradient is applied along the Y-axis, the direction of the gradient field is along the Z-axis. The frequency difference in the neighboring protons results in a time/phase difference in the precession of the protons. Even when the phase encoding gradient is removed, the phase difference continues to persist. This phase difference at a particular location is proportional to the gradient strength at that location. Hence every point along the Y direction is encoded on the basis of the phase of the precession as shown in Fig. 7. Thus every location on the image data is uniquely encoded by frequency in the X-direction and by phase in the Y-direction. Note that the direction

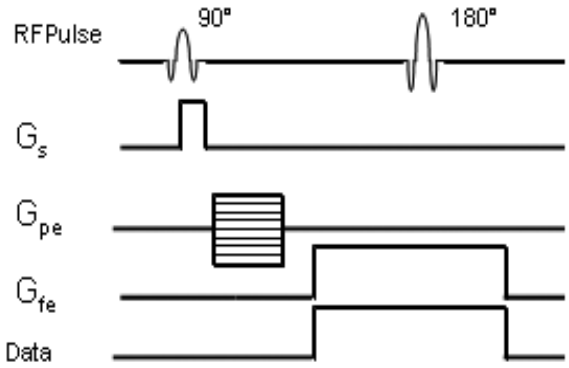

Fig. 8. A typical pulse sequence acquires k-space data. The image and the k-space data are related by the Fourier transform

of the frequency and phase encoding gradient can be interchanged. Signal localization is thus achieved with three gradients along the Z, X and Y direction.

5. Pulse Sequence and k-space Data

One line is traversed per phase encoding. Data along this line is then spatially coded and acquired during frequency encoding using a pulse sequence. A typical pulse sequence is shown in Fig. 8.

Data collected by a pulse sequence is called k-space data and shares a Fourier relation with the image required i.e., the image is the spectrum of the k-space data collected. Conventionally, the image is in the spatial domain but in MRI, the image is obtained in the frequency domain. This is because the image obtained is the Fourier Transform of the data collected from the scanner. To avoid confusion, the scanner data is said to be in k-space while the image is said to be in image domain or fourier domain. The MR signal is called echo.The time required to generate echo is denoted as the echo time TE. An echo is just a symmetrical FID obtained using the pulse sequence. One echo forms one line in the k-space (Fig. 9). The time required to

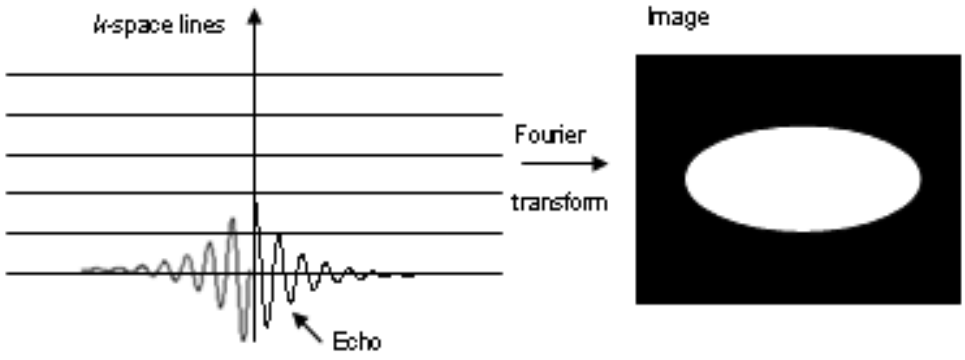

Fig. 9. One echo is one line in k-space

acquire one line of k-space is called as the repetition time TR. To acquire N lines in k-space, the pulse sequence shown above has to be repeated N times. The total time required to acquire the whole image data t_{acq} is given by

$$t_{acq} = N \times TR \tag{1.7}$$

Hence the total imaging time in MRI depends on TR and N.

CHAPTER II

RAPID MAGNETIC RESONANCE IMAGING

Typically a MR scan takes at least 20 minutes and can go on for an hour or more. Rapid imaging of biological structures gives a detailed understanding of the tissue dynamics and an insight into the operating mechanism of different human systems. For example, imaging of the heart in real-time can provide an insight into cardiac dynamics, facilitating knowledge about its operation in normal conditions and in case of an abnormality. Also of great importance is the imaging of blood flow through the body and the study of brain function. The applications mentioned above demand extremely fast imaging modalities.

Imaging has to be quicker than the fastest tissue velocity encountered. Any tissue motion causes a blur in the resultant image. For image analysis to detect abnormalities, temporal resolution has to be increased while maintaining the required spatial resolution. This poses a big challenge for pulse-sequence design and gradient system design.

A. Imaging Time Reduction Methods in MRI

As seen earlier, the total imaging time in MRI depends on the repetition time TR and N. TR in turn depends on the tissue relaxation times $T1$ and $T2$. The protons excited during the acquisition of one line have to completely relax back before the second acquisition and excitation begins so that the MR signals generated, do not mix. This wait period is also essential for higher signal strength.

Attempts are made to increase the imaging speed by reducing TR to an acceptable limit or by reducing the acquisitions (or excitations) required for the entire image data-set. New pulse sequences have been designed for this purpose.

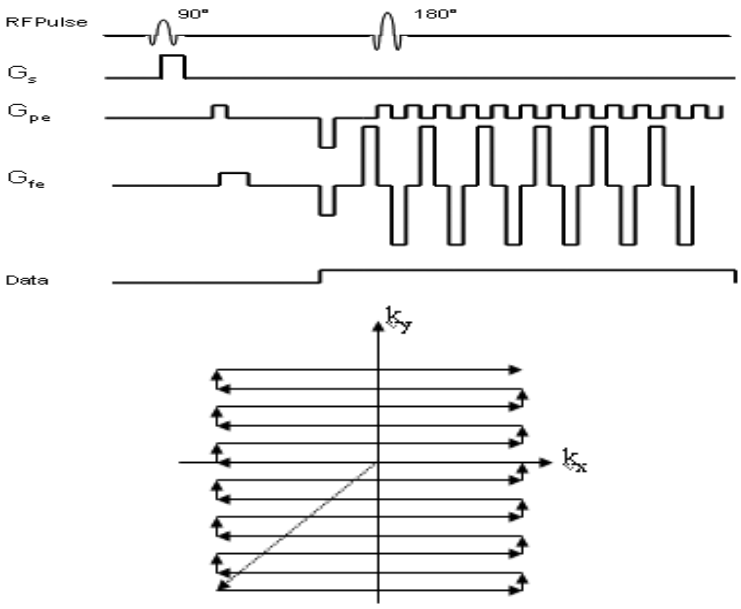

Fig. 10. The EPI pulse sequence (above) and EPI kspace coverage (below).

1. Pulse Sequences

Pulse sequences have been designed for rapid imaging since 1977 when a pulse sequence called Echo Planar Imaging (EPI) was developed for flow measurement[3].

a. Echo Planar Imaging (EPI)

EPI was used for real-time cardiac imaging in 1987 [17] bringing down the image scan time to 40msec with a resolution of 4mm. TR as seen earlier, is time between two acquisitions. This pulse sequence aims at reducing the time elapsed between two simultaneous acquisitions. The pulse sequence and the k-space coverage for EPI is shown in Fig. 10. Improvements such as segmented or interleaved EPI [7] have been developed to improve the resolution to 2.6mm for 110msec of scan time. However, an EPI sequence is extremely difficult to implement practically. It is limited by the current hardware and the gradient switching speed. Some of the disadvantages of

EPI are

1. *Gradient systems:* It is hard to get the correct gradient rise times for rapid switching.

2. *Eddy currents:* The gradient switching generates eddy currents in the MR hardware system and show up as artifacts in the image in the form of bright spots.

3. *Field inhomogeneity:* Any spurious gradients generated due to the inhomogeneities in the $\vec{B_0}$ cause artifacts in the resultant image.

4. *Chemical shift:* This is the shift in the resonance frequency of the proton in two different chemical environments. For instance, the hydrogen protons in water and fat show a difference of around 3ppm due to the different molecules they are surrounded by at 1Tesla. This effect becomes more pronounced with higher gradients.

b. Fast Spin Echo (FSE)

Fast Spin Echo is another pulse sequence used to facilitate rapid imaging. This sequence collects more lines per echo unlike the convention where only one line is collected for every RF excitation. Out of N k-space lines to be collected, if M lines are scanned per echo then the total acquisition time is reduced by N/M. The M lines collected per excitation are selected far away from one another so that their signals do not mix. The pulse sequence and the coverage is as shown in Fig. 11. FSE has the following drawbacks:

1. *Excess RF power:* For acquiring multiple lines, multiple 180° pulses have to be applied causing a lot of RF power to be accumulated on the subject being imaged. The magnetization starts saturating and the signal strength decreases.

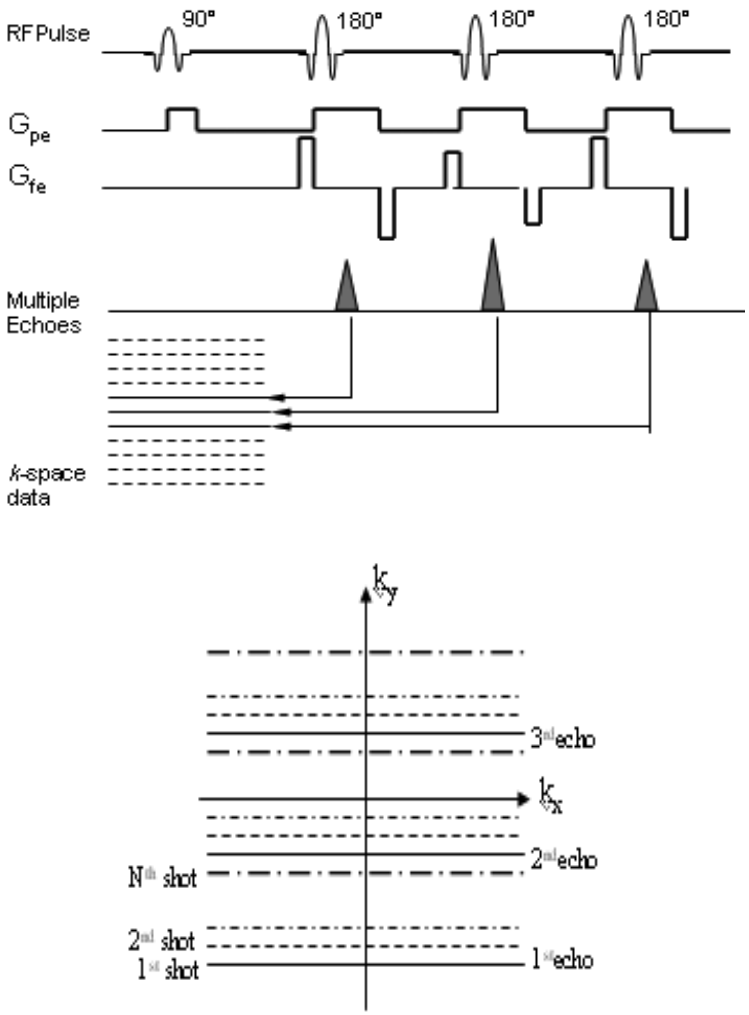

Fig. 11. The FSE pulse sequence (left) and the FSE k-space coverage (right)(Figure modified from [15]).

2. *Different TE problem:* Since the M lines are acquired at different times, each line in reality corresponds to a line from an image acquired at a different TE. The reconstructed image therefore corresponds to an approximate TE and may cause blurring.

3. $T2$ *decay:* As the phase encoding gradient applied for collection of each of the M lines is after considerable time gap, the T2 decay effect becomes prominent resulting in a blurring.

c. Other Pulse Sequences

Improvements over the above sequences like Interleaved EPI, Spiral EPI, RARE (Rapid Acquisition and Relaxed Excitation) [7] have been developed which offer increase in speed and increase in resolution. The image resolution can be improved to about 1.2mm with the Interleaved EPI. Sequences like true Fast Imaging with Steady-state Precession (FISP) [10] have also emerged for fast imaging which enhance the contrast of the image thus improving image quality.

All pulse sequences collect all N lines in k-space but reduce TR. Further advances in rapid imaging are made possible by parallel imaging where N is reduced.

2. Parallel Imaging

Parallel Imaging developed as a complementary technique for reducing the image scan time, using locally sensitive multiple receivers. The total number of phase encodings are reduced to decrease imaging time. The image is reconstructed using information in the form of the coil sensitivity profiles to compensate for the lesser data collected in k-space compared to the previously described techniques. This technique is explained in detail in the next chapter.

CHAPTER III

PARALLEL MAGNETIC RESONANCE IMAGING

Pulse sequences achieve considerable increase in the imaging speed. They mainly aim at reducing the TR. Parallel imaging aims at accelerating the imaging speed by reducing the number of k-space lines collected by the scanner.

From Fourier theory, most of the image information is stored at the center or in the lower frequencies in the frequency domain. Collecting a few lines in center of k-space can produce an image but it would not be useful for medical analysis. Parallel imaging therefore suggests different ways in which lesser k-space lines can be collected and yet a good image can be obtained for diagnosis. The number of lines reduced is determined by the reduction factor or acceleration and denoted by R. A reduction factor of 2 or an acceleration of 2 implies half the usual number of lines were acquired.

A. Basic Concept

Unlike a conventional MRI scanner, parallel MRI requires an array of receivers to collect data simultaneously. Thus each coil is only locally sensitive as shown in the Fig. 12. In other words, with a receiver placed near a subject, the signal contributed by the subject to the receiver varies according to the relative position of the subject from the receiver. Thus, though every receiver collects the same k-space data, each one contains different information about the image

In parallel MRI, data collected by each receiver element in k-space is subsampled data. Therefore, individual aliased images are obtained for every coil. These images are either unfolded in the image domain to yield the final image or the missed k-space lines are reconstructed using apriori information in the form of the spatially varying

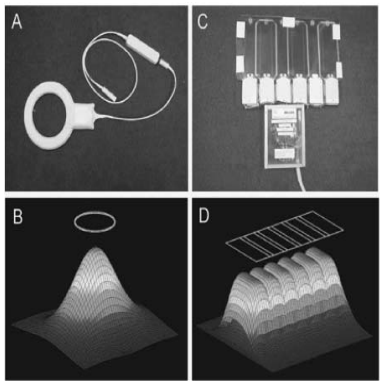

Fig. 12. A: Body coil for conventional MRI scan, B: Coverage of body coil, C: Array of receivers for parallel MRI, D: Coverage of the array, each acquired a fraction of the total image. [1]

coil sensitivity distribution.

Consider for instance, two coils instead of the regular volume coil with sensitivities as shown in Fig. 13. Then each coil acquires only half of the image since it receives strong signal from areas it is closest to and low or no signal from points away from it. This effectively reduces the coil field of view (FOV) to half that of the image. If the individual coil data now were subsampled in k-space by a factor of 2, two halves of the image can be obtained simultaneously from the two coils. Once the two images are appropriately reconstructed after data acquisition, they can be combined to get the entire image. Various algorithms have been developed for correct image reconstruction and can be classified [11] as

- *Image domain based reconstruction:* Reconstruction is done by unfolding every image using the coil maps. For e.g., SENsitivity Encoding (SENSE) [9], Partially Parallel Imaging with Localized Sensitivities (PILS) [12].

- *K-space based method:* Reconstruction is done by regenerating the missed k-space lines either for the ideal image or for individual coil images. For e.g.,

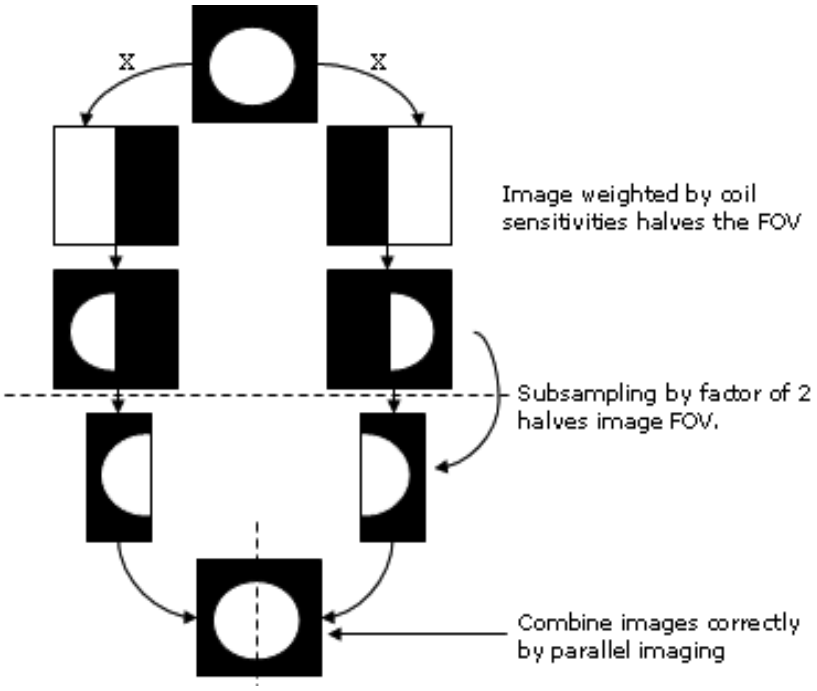

Fig. 13. Basic concept of parallel MRI

SiMultaneous Acquisition of Spatial Harmonics (SMASH) [4], Autocalibrating SMASH (AUTO-SMASH) [14], Variable density AUTO-SMASH (VD-AUTO-SMASH) [16], GeneRalized Autocalibrating Partially Parallel Acquisitions (GRAPPA) [13].

- *Hybrid reconstruction:* Reconstruction is done partly in the image domain and partly in k-space. For e.g., Sensitivity Profiles from an array of Coils for Encoding and Reconstruction In Parallel (SPACE RIP) [20].

B. SENSE

Reduced FOV images are obtained using Parallel MR scanning. Since the reduction factor is already known, the overlap amongst the pixels in every coil image is known. The sensitivities of the each individual coil are estimated or available as apriori infor-

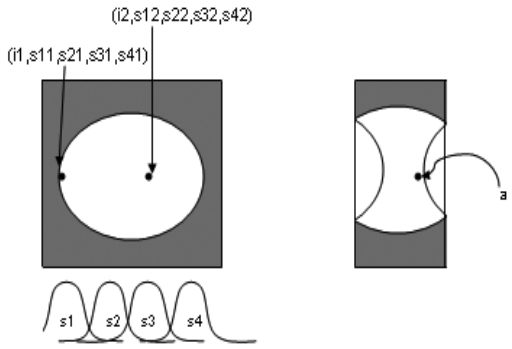

Fig. 14. Overlap of image pixels in SENSE

mation. A set of linear equations can be written down for every pixel in the reduced FOV using these coil profiles and overlapped image intensities to solve for the required image pixel values. In Fig. 14, for 4 coil data with reduction factor 2, consider aliased pixel 'a' in the reduced FOV for every coil. This pixel is the sum of the pixels at locations marked and weighted by the sensitivity of the coil at that location. If the image intensity at the two locations is i_1 and i_2 and the sensitivities of the 4 coils at the respective locations are s_{11}, s_{21}, s_{31}, s_{41} and s_{12}, s_{22}, s_{32}, s_{42}, then

$$a_1 = i_1 \times s_{11} + i_2 \times s_{12} \tag{3.1}$$

$$a_2 = i_1 \times s_{21} + i_2 \times s_{22} \tag{3.2}$$

$$a_3 = i_1 \times s_{31} + i_2 \times s_{32} \tag{3.3}$$

$$a_4 = i_1 \times s_{41} + i_2 \times s_{42} \tag{3.4}$$

where a_1, a_2, a_3 and a_4 are the intensities of the aliased pixels in the 4 reduced FOV individual coil images. Hence with a set of linear equations, the actual unfolded pixel values can be estimated.

C. Regularized SENSE

Reconstruction using SENSE gives a poor image due to inaccurate estimation of the coil geometry causing the reconstruction matrix to be ill-conditioned[6]. SNR is further reduced in SENSE due to this condition. Tikhnov regularization[21] is done to make use of the low resolution coil maps as apriori information. Error due to noise and ill conditioning is appropriately weighted using the regularization parameter λ. Selection of correct λ is important for noise suppression in Regularized SENSE.

$$I_{reg} = I_{rec} + (((S^H \times S + \lambda^H \times \lambda)^{-1}) \times S) \times (I_{prior} - S \times I_{rec}) \tag{3.5}$$

where I_{reg} is the regularized image, I_{rec} is the reconstructed image, S is the coil sensitivity matrix and λ is the regularization parameter.

D. PILS

PILS is based on the underlying assumption that the coils are highly locally sensitive. Therefore the coil FOV is very small as compared to the image FOV. No true aliasing occurs when individual coil data is subsampled. Knowing the coil center and its FOV, the exact location of the coil image can be determined, The unaliased image from the aliased data is cut and pasted in the correct location in the image FOV. PILS is sometimes also referred to as 'Scissors Method' for this reason. An illustration of the PILS method is depicted in Fig. 15. To cut the aliased images correctly, the coil sensitivities are approximated using a Gaussian function in order to determine the coil location in the entire FOV.

The entire PILS reconstruction can be summarized as follows [12]. For a coil with FOV F_c centered around c_0, the k-space can be reduced to the equation shown.

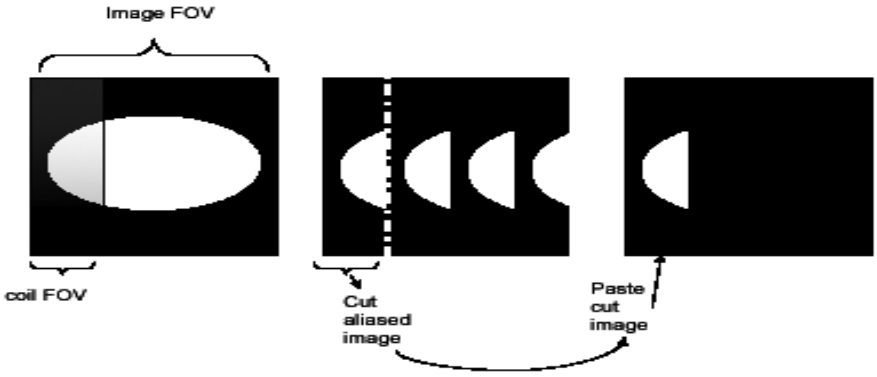

Fig. 15. PILS reconstruction

The integration is carried out only over F_c.

$$S(k_y) = \int_{F_c} \rho(y) e^{ik_y y} dy \tag{3.6}$$

.

Phase encoding direction is along Y-axis. $\rho(y)$ is the proton density of the sample being imaged. During reconstruction,the center of the coil c_0 is estimated from the sensitivity profiles. Hence the image can be reconstructed over a predefined area of range F_c as

$$\hat{\rho(y)} = FFT(\phi(k_y) S(k_y)) \tag{3.7}$$

where $\phi(k_y)$ determines the shift in the k-space data corresponding to a shift in the individual coil image according to the center of the coil. The point of maximum sensitivity is assumed as the center of the coil.

$$\phi(k_y) = e^{ik_y c_0} \tag{3.8}$$

The knowledge of the coil centers gives the relative position of the coils and hence a composite image can be formed.

E. SMASH

In SMASH, every skipped line is considered as data shifted in frequency from the nearest acquired line data. From Fourier Theory and the modulation property of Fourier transform, a frequency shift by ω_0 in the Fourier domain corresponds to multiplication by a sinusoid of frequency ω_0 in the image domain. For every missing line in k-space, a complex sinusoid is generated for the reconstruction. The complex sinusoids are generated by appropriate weighting of the coil profiles. The SMASH reconstruction can be explained with the following set of equations [4]. For a sample with proton density $\rho(x, y)$, coil sensitivity $C(x, y)$ and reduction along Y (phase encoding direction), the k-space equation can be written as

$$S(k_x, k_y) = \int\int dxdyC(x, y)\rho(x, y)e^{-ik_x x - ik_y y} \tag{3.9}$$

A complex sinusoidal of spatial frequency Δk_y^{comp} can be constructed as

$$C^{comp}(x, y) = \cos \Delta k_y^{comp} y + i \sin \Delta k_y^{comp} y = e^{i\Delta k_y^{comp} y} \tag{3.10}$$

If this were the coil sensitivity instead of C(x,y), then

$$S(k_x, k_y) = \int\int dxdy\rho(x, y)e^{-ik_x x - i(k_y y - \Delta k_y^{comp})} \tag{3.11}$$

Hence the combined MR signal obtained from all the coils together is shifted in k-space by Δk_y^{comp}. This shift can be interpreted as a shift of an acquired line to produce a missed line offset by the same spatial frequency Δk_y^{comp} in the image domain.

F. Auto-calibrating SMASH (AUTO-SMASH)

SMASH required an accurate estimate of the coil sensitivity maps to generate the weighting coefficients for every coil which usually is not possible. In addition, noise

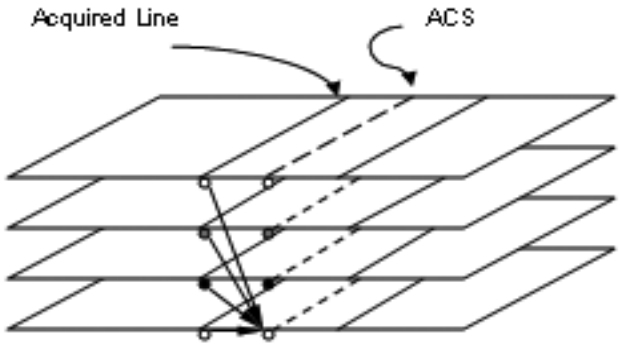

Fig. 16. Use of ACS lines in VD-AUTO-SMASH

in the k-space data causes error in the estimation of the weights. To avoid the process of sensitivity estimation, a few extra lines are collected called the Auto-Calibration Signal (ACS) lines. These lines are used to calculate the weighting coefficients required for image reconstruction. For a reduction factor of R, R-1 extra lines are required for AUTO-SMASH reconstruction. This does not significantly increase the imaging time. Besides eliminating sensitivity estimation, this approach also helps reduce motion artifacts and reduce sensitivity to noise.

G. Variable Density AUTO-SMASH (VD-AUTO-SMASH)

For better robustness and noise insensitivity, the reconstruction coefficients for each line are calculated using the ACS and acquired lines from all coils unlike AUTO-SMASH where reconstruction coefficients for a coil are calculated from data of the same coil. The process is illustrated in Fig. 16. VD-AUTO-SMASH results in acquisition of more ACS lines since a set of linear equations is now required to be solved.

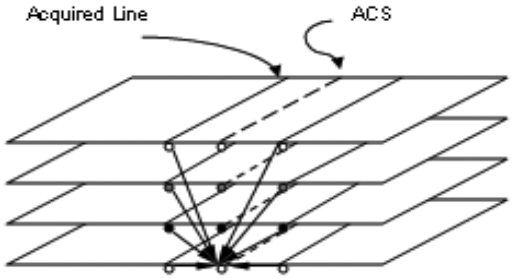

Fig. 17. Use of ACS lines in GRAPPA

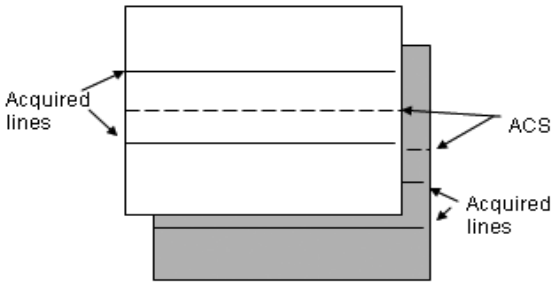

Fig. 18. Sliding blocks in GRAPPA

H. GRAPPA

GRAPPA further extends VD-AUTO-SMASH by considering more acquired lines per ACS line to determine the weighting factors as shown in Fig. 17.

This results in further immunity to noise and also makes the reconstruction less susceptible to motion artifacts. GRAPPA in its basic form is VD-AUTO-SMASH. It can be extended to reconstruct the image in different ways by using different acquired lines to generate the same ACS lines. In this case, SNR is calculated for every image and the weighting coefficients are weighted according to the SNR obtained. This approach is called the sliding block approach (Fig. 18).

I. SPACE RIP

SPACE RIP is a hybrid reconstruction method that first takes a inverse FFT along the frequency encoding making the rows/columns along the phase encoding direction, independent of each other. For every column, the k-space data is a FFT weighted by the coil sensitivity matrix. The data obtained for every coil can be written as (modified form [20]):

$$S_m(k_y, x) = \sum \rho(x, n) W_m(x, n) e^{ik_y n\tau} \tag{3.12}$$

where $W_m(x, n)$ is the complex sensitivity profile of the m^{th} receiver array element. This expression is converted into matrix from combining the k-space data of all coils and then solved to obtain the required image. If there are M coils and N lines are acquired per coil then, to generate one column of the image, a size $(M \times N) \times P$ matrix has to be inverted, making the reconstruction cumbersome. P is the number of total phase encodings in case of a full FOV scan. But this method is not restricted by the coil configuration of the k-space sampling. Matrix size reduces as reduction factor increases and reconstruction becomes faster unlike other methods where reconstruction time increases according to the acceleration.

J. Single Echo Acquisition (SEA)

SEA[19] is a different parallel imaging technique from those discussed above. In all the previous methods, every coil collects the same k-space data. In SEA, every coil collects different phase encodings which, when put together, form the complete k-space data of the image. Only one excitation is required and each coil acquires one echo line or one k-space line. Therefore, the image size for a C channel array and N frequency encodings will be $C \times N$. The required image is obtained by just a

simple inverse Fourier transform. The current research focuses on parallel imaging techniques in which all coils collect the same k-space lines.

CHAPTER IV

CHARACTERIZATION AND COMPARISON OF PARALLEL MRI TECHNIQUES

All parallel MRI techniques use similar k-space coverage but reconstruct the image differently. The image acquired therefore, depends on a number of factors discussed below.

A. Factors Affecting Parallel MR Reconstruction

The following factors affect the quality of the reconstructed image in parallel MRI:

Coil Configuration: Broadly, the coil arrays for parallel MRI are classified based on their spatial sensitivity profiles as:

Linear Array: Individual array elements are arranged one after the other in a plane. The phase encoding direction is fixed as the direction of differential sensitivities, i.e., the direction along which the coil sensitivities vary. Their sensitivity profiles are ideal for all parallel imaging reconstruction algorithms since the sensitivities vary spatially along one dimension and are uniform along the other.

Non-Linear Array: Array elements are arranged around the object to be imaged as if in a circle. The phase encoding direction can be arbitrarily chosen and may depend on the subsampling factor.

Most techniques are independent of the coil configuration but the coil arrangement has to satisfy different requirements for every reconstruction. For instance, PILS requires coil sensitivities to be extremely localized. The localization becomes an important criteria for this reconstruction since no true aliasing should occur even in the reduced FOV images. Specific arrangements of the non-linear arrays can also allow for PILS reconstruction. SMASH reconstructs the images by generating smooth

spatial harmonics by weighting the coil sensitivities. The coil profiles must be suitable to generate smooth sinusoids to generate a non-aliased image. Generally, linear arrays elements have gaussian or bell like profiles which make them suitable for SMASH. On the other hand, GRAPPA does not make use of the coil sensitivities directly. So the coil array type does not matter in the reconstruction. However, the placement of coils in a non-linear array may or may not cause aliasing artifacts to appear. SENSE and SPACE RIP also are relatively independent of the configuration of the coils, but depend on the correct estimation of the sensitivities. The noise varies from pixel to pixel and adjacent pixels are correlated. Therefore, it does not have a common-square root-dependence on the number of pixels [9].

Reduction Factor: Theoretically, the reduction factor is limited by the number of coils. Practically, reconstruction with reduction factor of above half the number of coils is poor. Noise, inaccurate estimation of sensitivity profiles, ill-conditioned reconstruction matrices, etc. restrict the reduction factor.

Coil Geometry Factor 'g': All reconstructions in parallel MRI depend on the spatial coil weightings, especially SENSE. As mentioned above, noise in the sensitivity information and correlation between pixels adversely affects image reconstruction. The geometry factor describes the ability of the coil to separate the aliased pixels accurately. A value of 1 indicates that the coils are ideal for reconstruction. Any value above 1 indicates deterioration in the reconstruction. The 'g' factor for the ρ_{th} pixel can be calculated as

$$g_{\rho,\rho} = \sqrt{diag((S^H \times \psi \times S)^{-1} \times diag(S^H \times \psi \times S))} \tag{4.1}$$

where S is the sensitivity encoding matrix and ψ is the noise correlation matrix. Ideally, the noise correlation matrix should be an identity matrix indicating no correlation amongst adjacent channels.

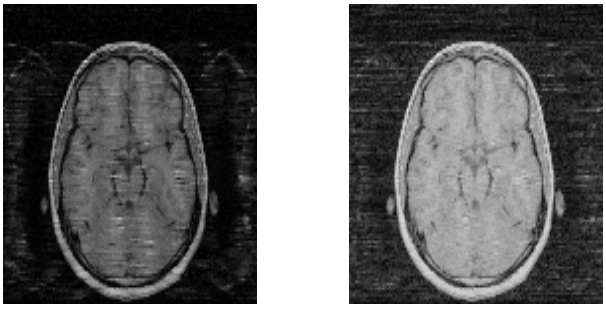

Fig. 19. Left: Image with usual SENSE reconstruction, R=4, 15 central lines, Right: Image with iterative SOS reconstruction.

K-space coverage: The acquired k-space lines can be uniformly sampled or the sampling density can be increased in the center of k-space. The extra lines can be used for sensitivity estimation but not in the actual reconstruction. GRAPPA and SPACE RIP make use of these lines in the reconstruction and can give a better image. An iterative Sum-Of-Squares(SOS) reconstruction [8] can also be done to incorporate the extra lines in the other methods after the main image is reconstructed. The improvement is seen in Fig. 19.

B. Performance Analysis

No one method has been picked as the method giving the best image under all conditions For a given imaging environment comprising of the factors mentioned above, the quality of the reconstructed image can be evaluated on the basis of:

1. Signal to Noise Ratio (SNR)

SNR is calculated using three different methods. The first method, which is the most convenient method to calculate, is a measure of how much the signal exceeds the

background intensity.

$$\text{SNR} = \frac{S}{SD} \tag{4.2}$$

S is the mean signal intensity in region of interest and SD = standard deviation in region of noise.

In parallel imaging, signal and noise are treated differently by different techniques. So the background noise cannot be assumed to be uniform and may lead to erroneous calculations, off by even 60% of the actual value. This may cause misinterpretation of data. A better way of calculating SNR is pixel-wise [12]. The pixel-wise SNR is calculated as:

$$\text{Pixel-wise SNR} = (\frac{S_{p,N}}{SD_{p,N}}) \tag{4.3}$$

$S_{p,N}$ is the mean signal intensity at pixel 'p' over 'N' acquisitions and $SD_{p,N}$ is the standard deviation at pixel 'p' over 'N' acquisitions Another way of calculating SNR in the true sense is using two acquisitions [2] as follows:

$$\text{SNR} = \sqrt{2}\frac{S_1}{SD_{1-2}} \tag{4.4}$$

S_1 is the mean signal intensity in ROI of any one image and SD_{1-2} is the standard deviation in the region obtained by the subtraction of the ROIs of the two images.

2. Artifact Power

The Artifact Power is a measure of how much signal power is spent in noise. Ideally all the signal energy would be concentrated in the object being imaged with the background being zero. Artifact power is the mean squared error between the reconstructed and the reference image. Practically, noise surfaces in the background and also in the region of interest, distorting the ideal values required. This error is

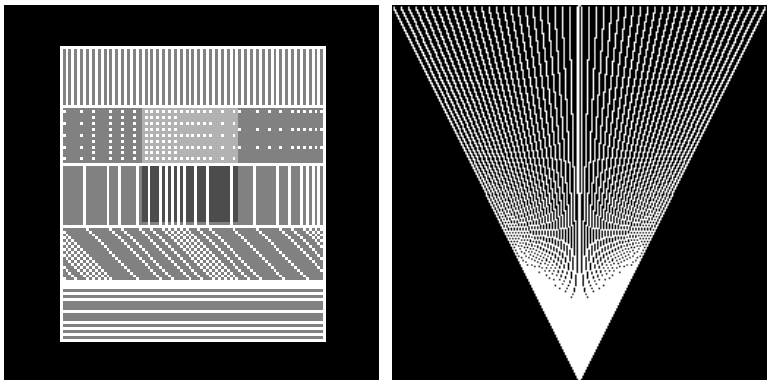

Fig. 20. Resolution phantoms

measured in terms of artifact power [12] as

$$\text{Artifact Power} = \frac{\sum[I_{reconstructed}(x,y) - I_{reference}(x,y)]^2}{\sum I_{reference}(x,y)^2} \tag{4.5}$$

3. Resolution

Since MRI is a not a linear time invariant system, the resolution cannot be represented by a simple convolution with a point spread function. Instead the point spread function can be evaluated at every pixel by using a point image and reconstructing the image using the parallel MRI reconstruction algorithms. For a typical 256×256 image, this procedure will be repeated 256^2 times. Since the resolution degrades in the direction of reduction or in the phase encoding direction, line spread functions can be studied by using 256 line images for the image reconstruction. To avoid this cumbersome procedure, a resolution phantom has been designed to take into account all possible ways to check deterioration in resolution. The resolution phantoms are as shown in Fig. 20.

Table I. Computations for 128×128 image with reduction factor R, n ACS and C coils (Additions and Multiplications are complex)

Method	Additions	Multiplications	IFFTs	Inverses
SENSE	$N^2(N-1)$	N^3	C	$1(N \times N)$
PILS	CN^2	$C\frac{N^2}{R}$	C	–
SMASH	$2C(N-1)+$ $\frac{N^2}{R}(C-1)$	$C(2+\frac{N}{R})$	1	$R(N \times C)$
GRAPPA	$n\frac{N^2}{R}+$ n^2N+CN^2	$(n-1)(\frac{N^2}{R}+nN)$	C	$N(n^2+2or4)$
SPACE RIP	$C\frac{N^3}{R}$	$\frac{N^3C}{R}$	$\frac{N^2C}{R}$	$N(\frac{N^2C}{R})$

4. Computations

The computational complexity of the parallel MRI techniques under consideration, can be evaluated on the basis of the number of IFFT operations performed, the matrix size and number of inverses computed, complex additions and subtractions. Consider an image of size $N \times N$, reduction factor R and number of coils equal to C and n calibration/ ACS lines, the computations are shown in table I. The computation time mainly depends on the code written and its optimality. GRAPPA and SPACE RIP are computationally intensive as compared to SENSE, PILS and SMASH. SMASH takes longer for a non-linear array where it has to perform an optimization to estimate the coil location.

CHAPTER V

SIMULATION AND EXPERIMENTAL RESULTS

A. Software Tool

In order to compare the parallel imaging techniques, all the algorithms and the performance analysis metrics were implemented in MATLAB. A software tool has been developed to incorporate all these parallel MR reconstruction techniques and their evaluation. A part of the Graphical User Interface (GUI) is as shown in Fig. 21. The

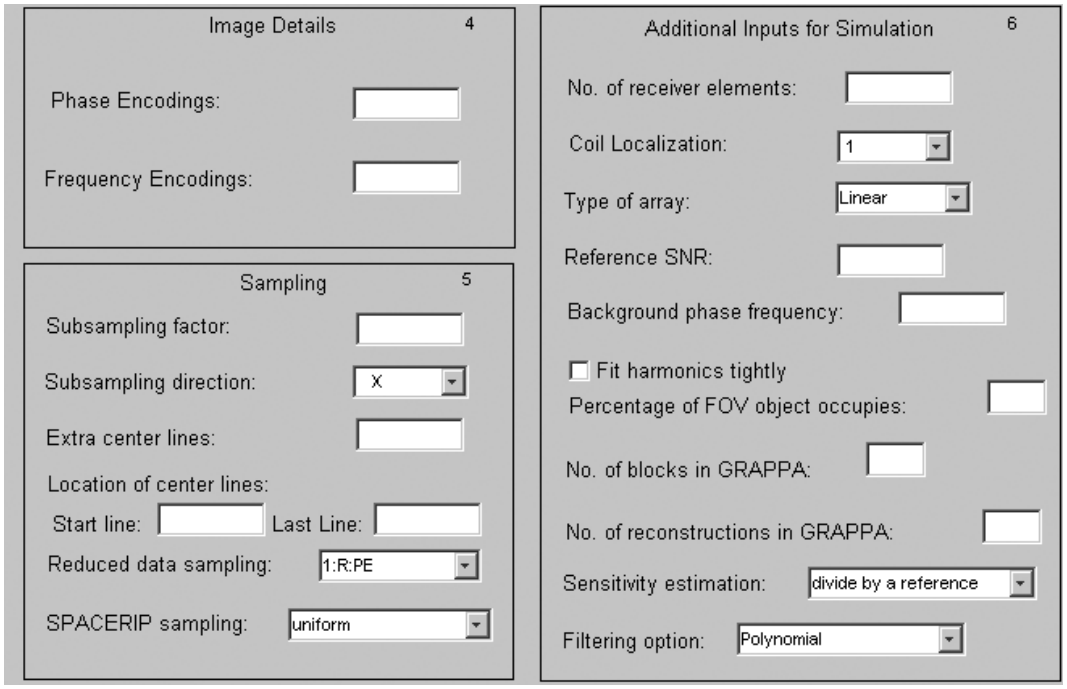

Fig. 21. The GUI

use of the tool is through 6 major steps listed below.

Data Input: Simulated data or raw data acquired from the machine is input to the software. Simulated data can be any image, not necessarily a medical image.

Then coil sensitivities are generated as per the user specifications. To simulate the coil sensitivity variation of a linear array, a 1D gaussian profile is generated. To simulate the variation of sensitivities for a non-linear array of coils, 2D gaussian patterns, covering the entire image FOV, are generated. K-space data are then simulated from the image and coil maps. Reduced data-set is obtained by retrospectively decimating the data by the user specified reduction factor. Care is taken to include the line corresponding to DC while reducing k-space since it contains maximum information.

File Inputs: The file containing the data is entered next. Extra calibration data required for sensitivity estimation is also entered. The files must be in the '*.mat' format. For calibration data, the location of the lines must be known and entered. A body coil image can also be used instead of the low resolution Sum-Of-Squares (SOS) image to improve the estimation of sensitivities. If an image is input for simulation, it may be a bitmap (*.bmp), portable network graphic (*.png), or JPEG image.

Sensitivity Estimation: The sensitivity estimation process can be effected using:

Divide by body coil image: Individual full FOV coil images are obtained. Each pixel in these coil image is divided by the corresponding pixel in the body coil image.

Self-Calibration: The self-calibration technique makes use of a few more lines acquired after the main scan called ACS. Coil profiles can be calculated by a simple divide by sum-of-squares (SOS) image as in the previous method. Using the ACS lines, low resolution full FOV images are obtained. Division of each low resolution full FOV image by the SOS image gives the sensitivity maps. Coil spatial weightings can also be calculated using the Walsh method using singular value decomposition [5].

Noise Suppression: The toolbox incorporates noise filtering techniques to enable suppression of the noise that appears while reconstructing the picture of the object

using coil maps. For noise filtering, the toolbox provides variable order and variable neighborhood polynomial filters. Median filtering can also be used. To avoid Gibb's ringing, windowing is done regardless of whether the filters are used or not.

Image Reconstruction: SENSE, Regularized SENSE, PILS, SMASH, AUTO-SMASH, GRAPPA, SPACE RIP are implemented in the toolbox. The tool also provides iterative SOS reconstruction, which makes use of the ACS line in the final reconstructed image.

Evaluation of Reconstructed Image: The methods are evaluated on the basis of parameters mentioned in Chapter 4. SNR and artifact power are primary in determining the performance of the reconstruction algorithm. The first method of SNR calculation is used for the comparison since multiple acquisitions were not available. Simulations for resolution, and pixel-wise SNR were done and the results are shown later in this chapter. The block diagram of the tool-box showing the data flow is illustrated in the Fig. 22 [18].

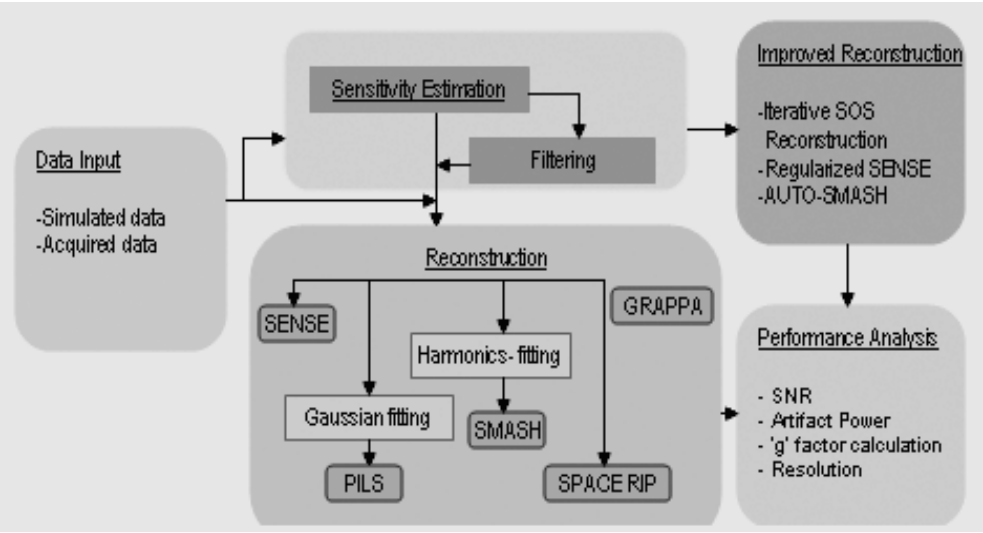

Fig. 22. Block diagram of the toolbox

B. Results Based on Actual and Simulated Data

Reconstructions were performed using 3 coil stomach data, 8 coil linear array spine data, 8 coil non-linear array head data and 64 coil phantom data. During the process of testing and optimization, synthetic simulations were performed on the MRI phantom available in MATLAB.

1. Three Coil Data

A dataset for three non-linear coils was reconstructed using the five basic methods and compared for SNR (method 1) and for artifact power. Since multiple acquisitions were not available, SNR by the other two methods cannot be evaluated. 16 lines in the center of the k-space were collected, reducing the reduction factor to 1.7777. The reference image is shown in Fig. 23. The actual reconstructions for SENSE, PILS, GRAPPA and SPACE RIP are shown in Fig. 24. The comparison charts are shown in Fig. 25.

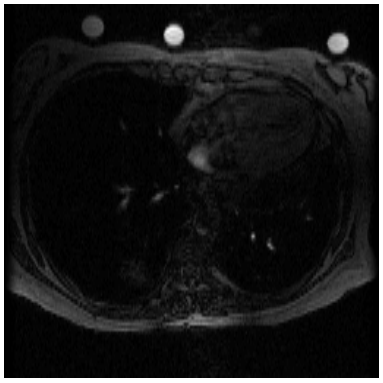

Fig. 23. Reference image for the 3 coil data.

SMASH Reconstruction caused aliasing and hence was not used for comparison. GRAPPA has the maximum SNR and the minimum artifact power for the three coil

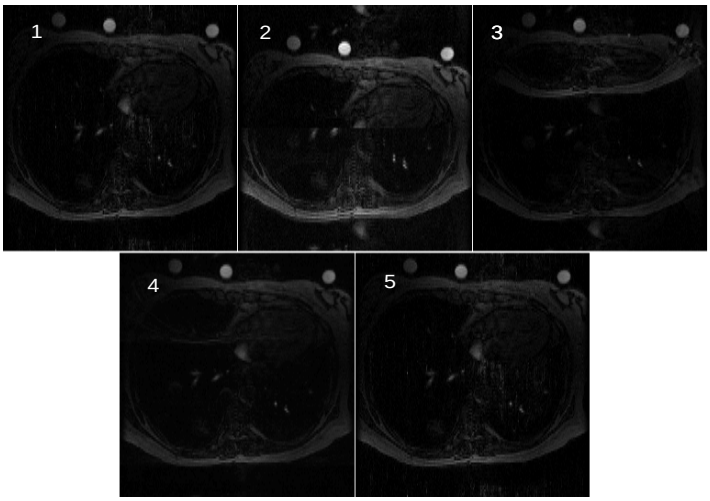

Fig. 24. Image reconstruction for the 3 coil non-linear array data (1: SENSE, 2: PILS, 3: SMASH, 4: GRAPPA, 5: SPACE RIP).

data set. The PILS image looks better than the rest but careful observation reveals that the image got cut in the center compressing the image a little. This error was due to incorrect estimation of the coil centers. The artifact power is very high due to this reason. In terms of overall image quality, GRAPPA is the best scheme, followed by SENSE and SPACE RIP.

2. Eight Coil Data for a Linear Array

a. Reduction Factor of 2

For the 8 coil dataset with the elements arranged in a linear array, a reduction factor of 2, 16 center lines were collected for self calibration. Since the coil arrangement is such that only two out of the 8 coils span 70 percent of the total image FOV, SMASH does not reconstruct the image properly as smooth harmonics cannot be generated. SENSE , PILS and GRAPPA provide a valid reconstruction for reduction factors of

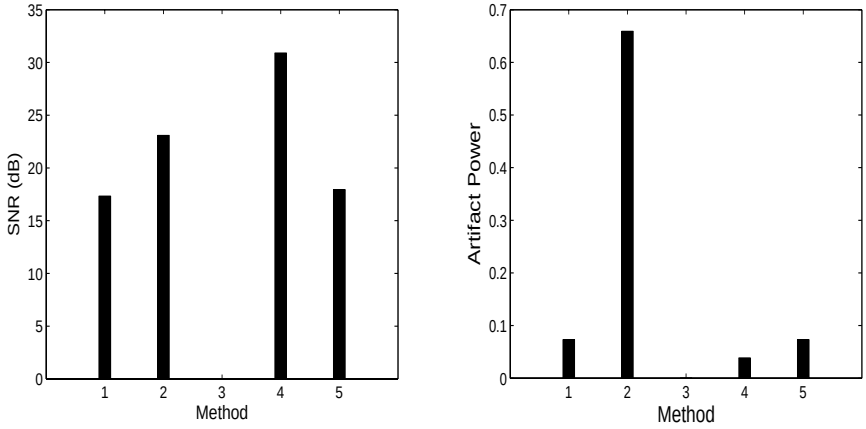

Fig. 25. SNR and artifact power for 3 coil non-linear array data, R=2, 16 center lines (X axis - 1: SENSE, 2: PILS, 3: SMASH, 4: GRAPPA, 5: SPACE RIP) .

2, 3, 4. The reference image is shown in Fig. 26 while results for a reduction factor of 2 with 16 center lines are shown in Fig. 27 and Fig. 28.

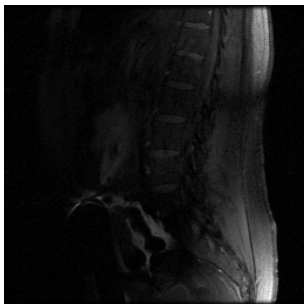

Fig. 26. Sum-Of-Squares image obtained from the full k-space data for the 8 coil linear array.

Increase in the number of self calibration lines may or may not lead to an improvement in SENSE and SPACE RIP but improve the GRAPPA reconstruction. More ACS lines are available and hence the reconstruction coefficients are more accurate resulting in a better image. The extra lines add to the imaging time and reduce the acceleration factor (subsampling factor) from 2 to 1.8823 for 16 center lines and

Fig. 27. Reconstructed images for 8 coil linear array, R = 2, 16 center lines (1: SENSE, 2: PILS, 3: GRAPPA, 4: SPACE RIP)

to 1.7777 for 32 center lines.

b. Reduction Factor of 3

Because of the non-uniform FOVs of the coil array elements, and noisy nature of the images obtained from the middle two coils, PILS reconstruction fails for a reduction factor of 3 (actual R = 2.4385). SENSE and SPACE RIP provide a better SNR than GRAPPA. The SNR is marginally lower in GRAPPA but the artifact power in GRAPPA is significantly less. The SNR calculation just provides a measure of the difference in the signal intensity and noise and not the SNR in the true sense.

The artifact power measures the squared error between the SOS reconstruction and the image obtained from parallel imaging. It is therefore, a better measure of the quality of the reconstructed image. Since GRAPPA has the least artifacts, the GRAPPA reconstruction is superior to the other reconstructions. The plot for the

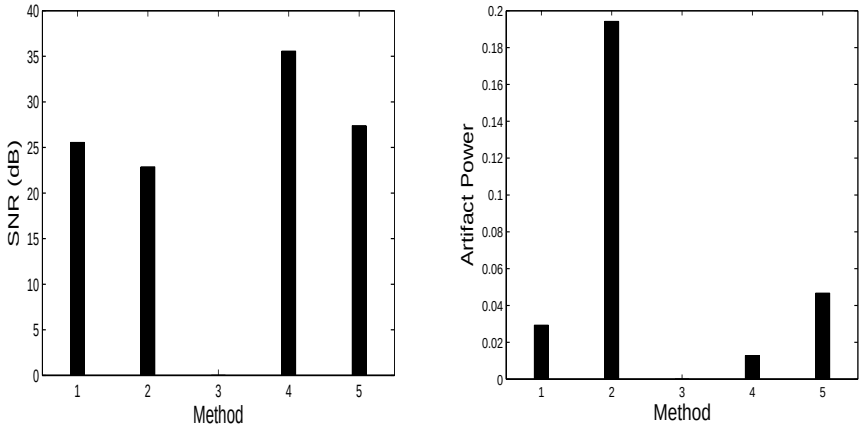

Fig. 28. SNR and artifact power for 8 coil linear array data, R = 2, 16 center lines (X axis - 1: SENSE, 2: PILS, 3: SMASH, 4: GRAPPA, 5: SPACE RIP).

SNR and the artifact power are shown in Fig. 29.

c. Reduction Factor of 4

For a reduction factor of 4 and 32 center lines (actual R = 2.9090) only SENSE and SPACE RIP reconstructions are valid since the other reconstruction methods fail to remove aliasing from the final image. For 48 center lines, GRAPPA reconstruction shows a higher SNR than the corresponding SENSE image. But the reduction factor then goes down to 2.6666. The reconstructed images are shown in Fig. 30.

We observe that, with 48 center lines as opposed to 32, the improvement in the GRAPPA reconstruction is significantly higher than that in the SENSE and SPACE RIP reconstructions. More lines in the center must improve the sensitivity maps. Acquisition of more calibration data in this case did not improve the SENSE image, indicating that the inherent coil data itself must be noisy. As can be seen in the images, the central two coil images are extremely noisy causing failure in reconstructing the image. GRAPPA smoothed out the noise effects. This is probably

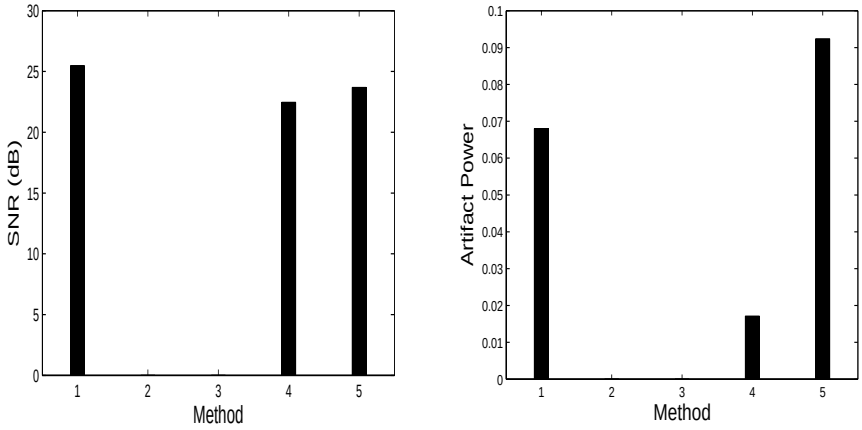

Fig. 29. SNR and artifact power for 8 coil linear array data, R = 3, 32 center lines (X axis - 1: SENSE, 2: PILS, 3: SMASH, 4: GRAPPA, 5: SPACE RIP).

because at the extreme phase encoding, the missed lines cannot be estimated correctly. There are no lines before the first phase encoding and after the last phase encoding line (See Fig. 17) and get set to nearly zero thus providing a kind of filtering to the noise.

3. Eight Coil Data for a Non-linear Array

For the non-linear array, PILS and SMASH failed to reconstruct the image even at a reduction factor of 2. Therefore, only SENSE, SPACE RIP and GRAPPA are compared. Similar results are obtained for the non-linear array data set.

a. Reduction Factor of 2

SENSE reconstruction showed a higher SNR and a lower artifact power when compared with the GRAPPA reconstruction with 2 blocks and the SPACE RIP reconstruction. With 4 blocks, SNR obtained in GRAPPA was still lower than in SENSE but the artifact power is significantly lower than the usual reconstruction.

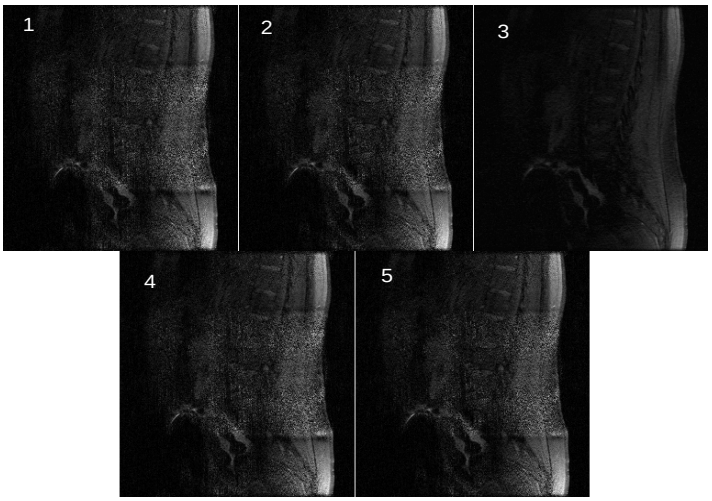

Fig. 30. Reconstructed images for a 8 coil linear array data, R = 4 (1: SENSE (32 center lines), 2: SENSE (48 center lines), 3: GRAPPA (48 center lines), 4: SPACE RIP (32 center lines), 5: SPACE RIP (48 center lines)).

For GRAPPA reconstruction, a 1D inverse FFT along the frequency encoding direction provided better results. The reconstructions and the comparison charts are shown in Fig. 31 and Fig. 32.

With 32 central lines , the artifact power reduced considerably in GRAPPA due to the availability of more ACS lines. Comparison bars for an acceleration factor of 3 are in Fig. 33. SENSE and SPACE RIP perform better than GRAPPA in this case. The aliasing artifacts may be eliminated by considering the correlation of samples along the frequency encoding direction, in addition to that along the regular phase encoding direction.

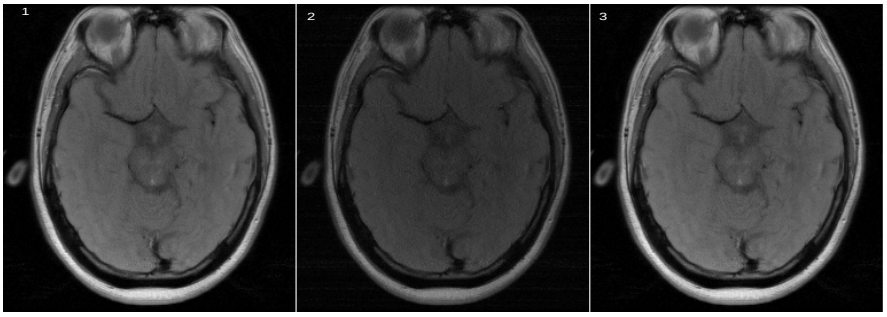

Fig. 31. Reconstructed images for a 8 coil non-linear array data, R=2, 16 center lines (1: SENSE, 2: GRAPPA, 3: SPACE RIP).

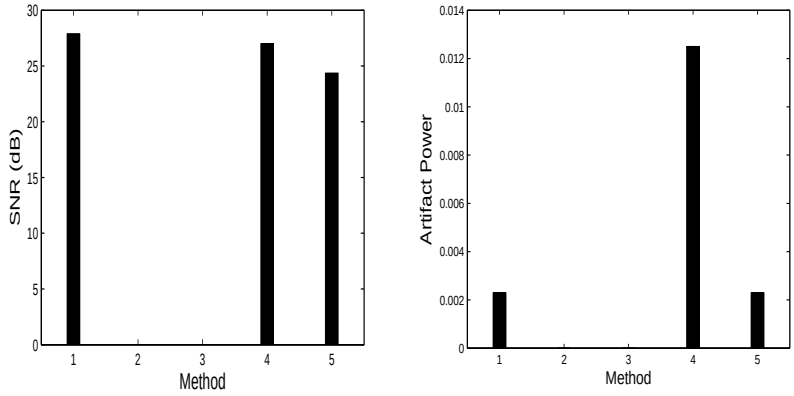

Fig. 32. SNR and artifact power for 8 coil non-linear array data, R = 2, 16 center lines (X axis - 1: SENSE, 2: PILS, 3: SMASH, 4: GRAPPA, 5: SPACERIP).

b. Reduction Factor of 3 and 4

With 32 center lines (actual R = 2.4380), SENSE, GRAPPA and SPACE RIP show approximately the same SNR but the artifact power for GRAPPA is significantly lower and hence GRAPPA can be regarded better than the remaining two methods. The comparisons for are illustrated in Fig. 34.

For a reduction factor of 4, GRAPPA reconstruction required 48 lines for a valid image. SENSE and SPACE RIP algorithms reconstructions were successful even for

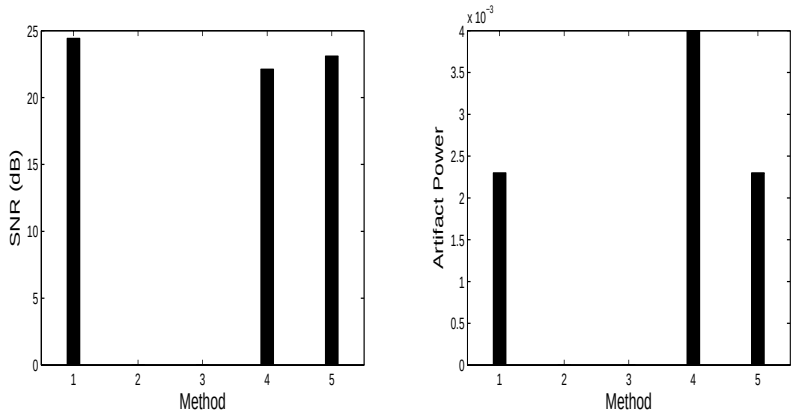

Fig. 33. SNR and artifact power for 8 coil non-linear array data, R = 2, 32 center lines (X axis - 1:SENSE, 2:PILS, 3: SMASH, 4: GRAPPA, 5: SPACERIP).

32 center lines with a low artifact power value. The results are shown in Fig. 35.

4. Sixty-four Coil Data for a Linear Array

Simulations were also carried out for a 64 channel linear array data-set.The data was reshaped to 256 240 to allow reconstruction with most of the reduction factors. Reduced data was obtained by retrospectively decimating the data according to the chosen reduction factor. Reduction factors as low as 2, 3, 4 and higher factors of 8 and 16 were tested. The coil-profiles of this data are designed to be extremely localized for capturing only one line's worth of information. The sensitivities overlap to acquire k space lines very close to one another to improve the resolution of the resulting image. In case of higher reduction factors, the number of center lines collected drastically reduces the effective reduction factor, R as seen in case of an acceleration factor of 8 and 16.Full encoded data-set for a phantom was acquired using the SEA array on a 4.7T system. Data for every coil was 256 256. Careful study of the k-space showed that the k-space data was not centered in the middle of k-space for all the coils. It was offset by about 10 lines. The phantom is shown in Fig. 36.

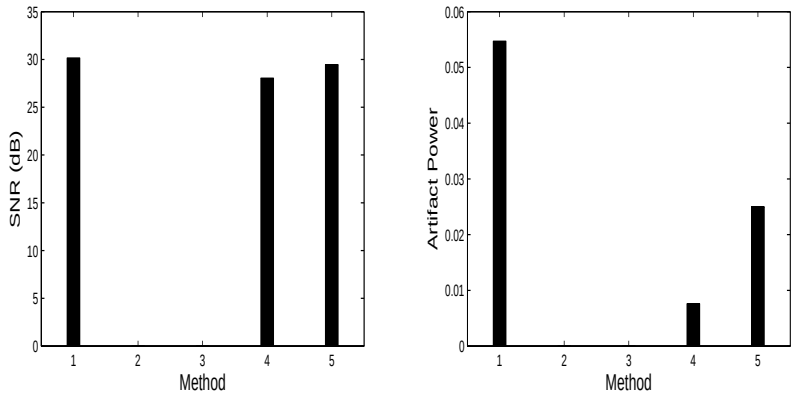

Fig. 34. SNR and artifact power for a 8 coil non-linear array data, R=3, 32 center lines (X axis - 1: SENSE, 2: PILS, 3: SMASH, 4: GRAPPA, 5: SPACE RIP).

a. Reduction Factor of 2

Since the coils are extremely localized, PILS provides the best reconstruction as expected. The comparison results for 16 center lines are shown in Fig. 37.

b. Reduction Factor of 3, 4 and Higher

Reduction factors of 3 and 4 are still small as compared to the number of coils used and PILS proves to be much better than the other reconstruction methods. However at higher reduction factors, aliasing artifacts become severe. SENSE and SPACE RIP provide poor reconstructions and GRAPPA provides blurred/ low resolution images. GRAPPA shows artifacts at low reduction factors but they are inherent in the coil data obtained . Appropriate number of lines, reconstructions and full flexibility of the reconstruction algorithm has to be tried out to get a good image. For a reduction factor of 4, the comparison bar graphs are shown in Fig. 38.

For a reduction factor of 8, 32 center lines were acquired but the overall acceleration factor drops down to 4 in reality. The SENSE and SPACE RIP images are similar. PILS and GRAPPA still provide a good reconstruction. The images are

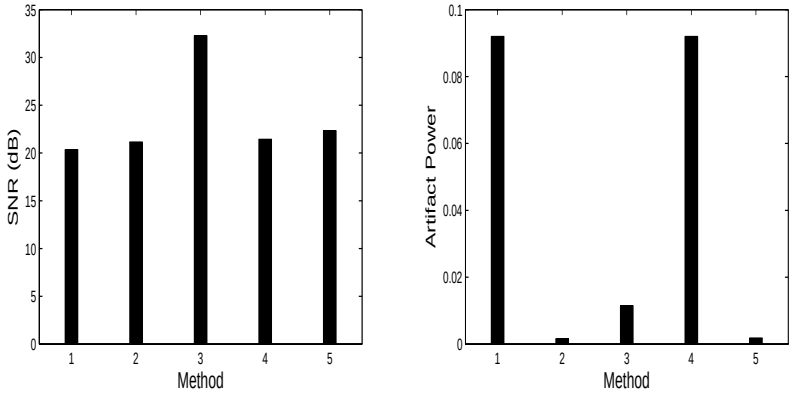

Fig. 35. SNR and artifact power for 8 coil non-linear array data, R = 4 (X axis - 1:SENSE (32 center lines), 2: SENSE (48 center lines), 3: GRAPPA (48 center lines), 4: SPACE RIP (32 center lines), 5: SPACE RIP(48 center lines)).

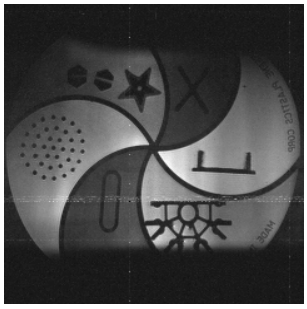

Fig. 36. Phantom image from the 64 channel linear array data

shown in Fig. 39 and the corresponding comparison is available in Fig. 40.

5. Simulated Data

Pixel-wise SNR requires atleast 40 to 50 simulations for accurate measurements. Practically only one acquisition is available but multiple acquisitions can be easily simulated. Accurate SNR at every pixel location is obtained using this method. The pixel-wise SNR maps for a reduction factor of 2 are shown in Fig. 41. The SNR maps

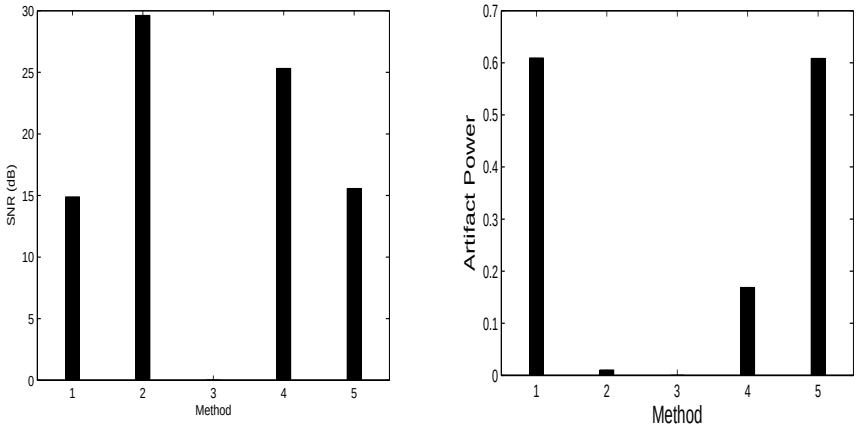

Fig. 37. SNR and artifact power for 64 channel linear array, R = 2, 16 center lines (X axis - 1: SENSE, 2: PILS, 3: SMASH, 4: GRAPPA, 5: SPACE RIP).

show the aliasing pattern and the fall in the SNR in the folded regions in SENSE and SPACE RIP. The map of pixel-wise SNR for PILS show higher SNR in the entire object FOV but shows the aliasing artifact in the total FOV of the image though it is not visible in the actual reconstructed image. GRAPPA shows a very good SNR map with no aliasing artifact and a higher SNR in the object FOV, again scoring over the other methods. The results for the simulation for a 8 coil linear data, R=2 and 16 center lines are shown with comparisons for SNR by method 1 and 3 described in the previous chapter in Fig. 42. The two-acquisition method (method 3) is a more accurate method of calculating SNR than the two region method (method 1) and the discrepancies in the two methods can be very well seen in Fig.42.

The resolution maps also show that the contrast decreases in SENSE. Resolution could not be quantified but the degradation in terms of pixels can be found by the user by looking at the resolution phantoms. This method therefore, may not give an accurate answer. The reconstruction of ther esolution phantoms gives a good idea of where the resolution is bad. At higher accelerations, the edges show a slight blur while the features in the center of the FOV are easily discernible. The extremely localized

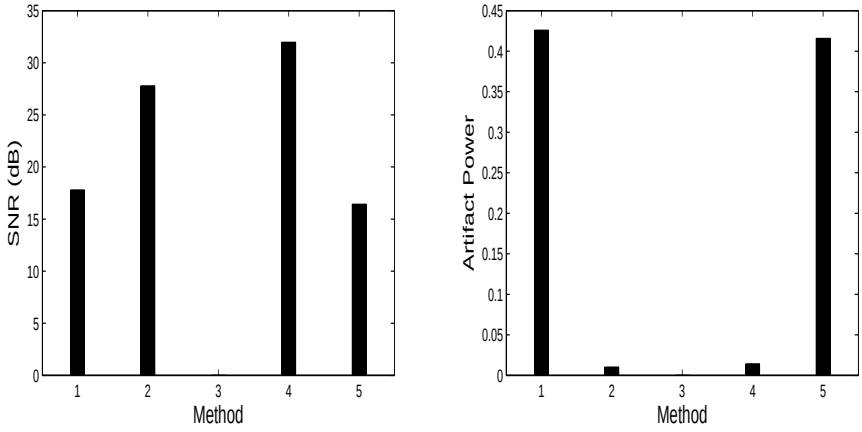

Fig. 38. SNR and artifact power for 64 channel linear array, R = 4, 32 center lines (X axis - 1: SENSE, 2: PILS, 3: SMASH, 4: GRAPPA 5: SPACE RIP).

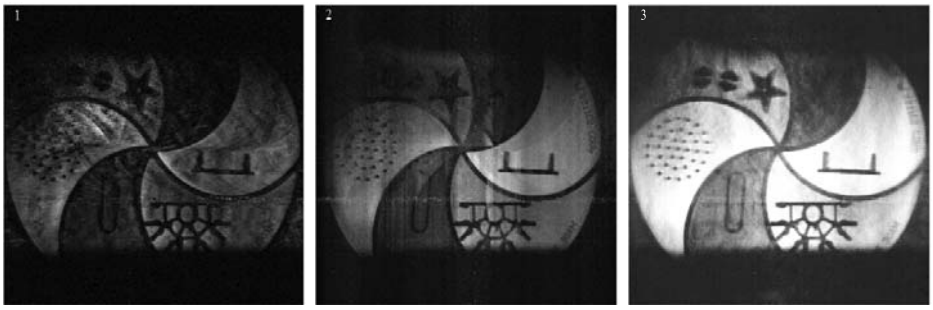

Fig. 39. Reconstructed images for 64 channel linear array, R = 8, 32 center lines (1:SENSE, 2: PILS, 3: GRAPPA).

nature of the coils in PILS provides a higher resolution than the other methods. In addition, it can be observed that the overall signal intensity in GRAPPA decreases but the contrast is maintained while in SENSE, contrast decreases.

The 'g' factor map are shown in Fig. 43. The bright areas show a value 1 meaning that pixels in these regions can be deciphered correctly. Other areas show a 'g' factor greater than 1 indicating the error in unfolding or inability of the coil to unfold the aliased pixels. (The map is inverted for better view). Regularized SENSE, an improvement over SENSE which has been implemented in this software

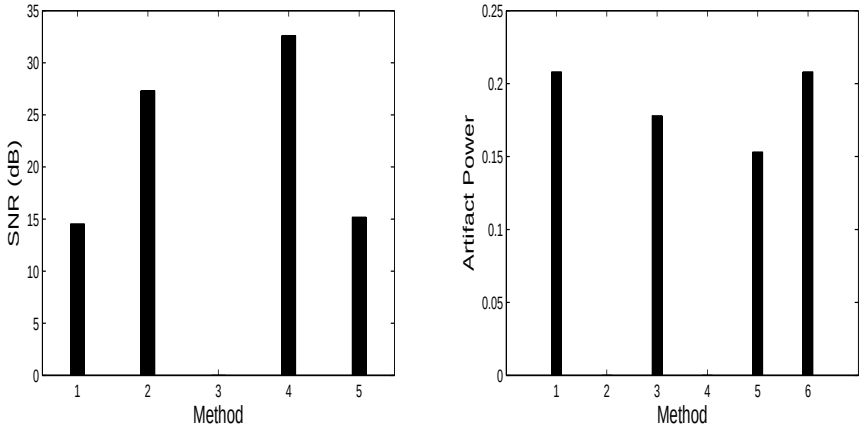

Fig. 40. SNR and artifact power for 64 channel linear array, R = 8, 32 center lines (X axis - 1: SENSE, 2: PILS, 3: SMASH, 4: GRAPPA, 5: SPACE RIP)

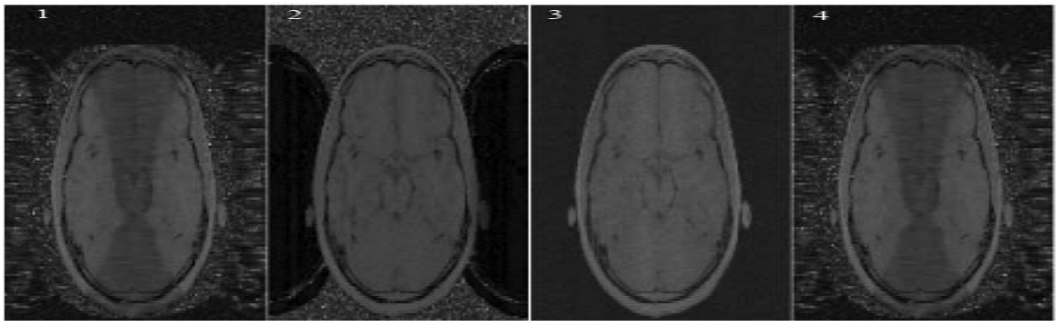

Fig. 41. SNR maps for 1: SENSE, 2: SMASH, 3: GRAPPA, 4: SPACE RIP

tool reduced the 'g' factor thus improving the ability of SENSE to unfold the aliased pixels correctly.

Extensive simulations on synthetic data and verification using acquired data was done and the five basic methods of SENSE, PILS, SMASH, SPACE RIP, GRAPPA were compared and analyzed for the same k-space data collected for every method. The comparison follows in the next chapter.

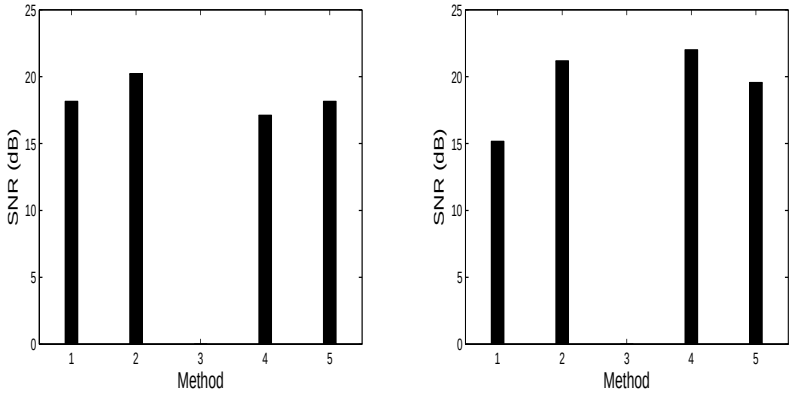

Fig. 42. SNR comparisons for method 1 and method 3(X axis - 1:SENSE, 2: PILS, 3: SMASH, 4: GRAPPA, 5: SPACERIP)

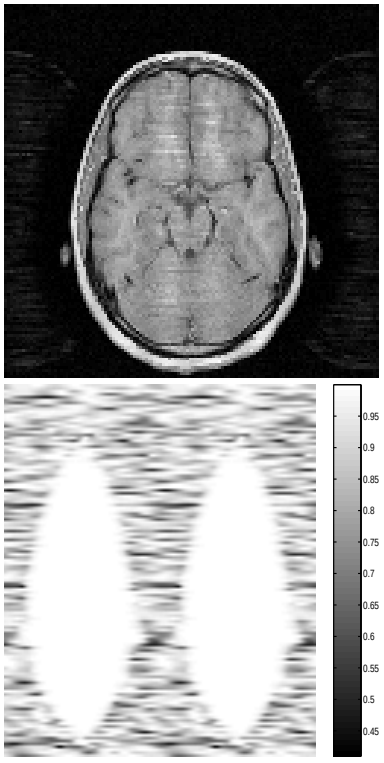

Fig. 43. SENSE image for R=2 and the corresponding 'g' factor map

CHAPTER VI

CONCLUSION

A software tool has been developed to study and compare the quality of the image, obtained using different reconstruction techniques in parallel MRI . Simulations were carried out on real and synthetic MR data. The optimal technique for image reconstruction depends heavily on the coil configuration, k-space coverage and reduction factor. Following are the conclusions drawn from this simulation and study.

GRAPPA offers flexibility in the choice of blocks, number of iterations and coil correlation to give valid results for any coil configuration. Reduction factors above 6 and sometimes even 4 are difficult to achieve practically, even with a large number of array elements. The study shows that higher reduction factors can be achieved using GRAPPA. Unless the specific constraints for a particular reconstruction technique are known to be satisfied, GRAPPA can always be relied on for an image reconstruction. For the 64 channel receiver, GRAPPA smoothed out the noise at high reduction factors to achieve a minimum norm solution giving a low resolution image where a least square solution failed to provide a valid reconstruction. This is true for the particular coil geometry of the receiver array, and k-space coverage but cannot be verified as a characteristic of GRAPPA. Signal intensity in GRAPPA decreases but the contrast is maintained while in all the other methods, contrast reduces. The acquired Auto-Calibration Signal (ACS) lines affect determination of the GRAPPA reconstruction coefficients which in turn depends on the underlying phase of the coil sensitivities. Using the simulation tool, various reconstructions for GRAPPA can be tried and the best one suited for a particular application can be selected.

Availability of accurate reference maps makes SENSE and SPACE RIP a better choice at lower reduction factors. They give a better resolution but lower contrast than

GRAPPA. However if a localized linear array of coils is available, PILS reconstruction may be preferred over all the other methods.

Computational complexity is one more way of evaluating the parallel MRI reconstruction techniques. It is important only in case of real-time applications like intra-operative imaging. Otherwise computational complexity can be given a lower priority. SPACE RIP and GRAPPA are computationally very intensive when compared to SENSE, PILS and SPACE RIP. SENSE therefore, becomes the optimum choice for applications requiring fast computational speed.

Image quality can be verified mainly on the basis of pixel-wise SNR and artifact power. SNR calculated by method 3 (using two acquisitions) is also reliable and hence priority must be given to these three performance parameters. Pixel wise SNR should be the most important factor in deciding the optimality of any of the parallel MRI reconstruction technique. The two-acquisition method and the artifact power evaluation corroborate the result obtained from a given imaging method.

The inferences for the data-sets studied and compared for this work can be summarised in the table II. The results are based on limited data available for this study and may not hold true for any new data set. For the comparison, more the stars better is the method. For sensitivity estimation, GRAPPa show a * since it does not require the coil profiles and hence is better than the other methods. AUTO-SMASH, the modified version of SMASH does not require sensitivity estimation but this comparison includes the original SMASH reconstruction. Only SPACE RIP can handle non-uniorm k-space and hence has a star while the others show a -. Non-uniform sampling of the k-space and corresponding SPACE RIP reconstruction was simulated and analyzed. The number of lines for non- uniform sampling were kept the same as for the uniform sampling. The reconstruction depends on the relative postion of the coils with respect to the object. For e.g., A set of 4 coils when placed two in

the anterior and two in the posterior may result in perfect GRAPPA reconstructions. The same 4 coils when positioned at 4 corners of the object FOV may cause aliasng in a GRAPPA reconstruction. Coil placements though not discussed in this work were tested using synthetis data. Results based on the simulation data are entered in this table. No one method can be selected as the optimum method but PILS and

Table II. Comparison of the five parallel MRI methods for the 4 data-sets.

	SENSE	PILS	SMASH	GRAPPA	SPACE RIP
SNR	**	***	*	$**\frac{*}{2}$	**
Contrast	*	**	*	**	*
Resolution	**	***	*	$*\frac{*}{2}$	**
Computation	*	*	$*\frac{*}{2}$	***	****
Artifact power	**	***	***	*	*
Low R	**	*	*	**	**
High R	*	*	*	**	*
Linear Array	**	**	*	**	**
Non-linear Array	**	*	*	**	**
Coil placement	*	***	***	**	*
Sensitivity estimation	–	–	–	*	–
Non-uniform k-space	–	–	–	–	*
Sensitivity to noise	**	**	***	*	**
Flexibility in reconstruction	–	–	*	**	*

SMASH fail to reconstruct the image under some imaging conditions. SENSE, SPACE RIP and GRAPPA provide a non-aliased valid image under most imaging set-ups.

The image quality generally varies greatly but as a thumb-rule, GRAPPA performs better for linear arrays and SENSE and SPACERIP perform well for non-linear arrays. GRAPPA seems to be comparatively unaffected by coil position. SENSE is completely insensitive to coil position but resulting image is usually very noisy while GRAPPA is insensitive to noise but computationally complex and so time consuming. Also as mentioned above, SENSE has better resolution and GRAPPA has netter contrast. A combination of these two techniques might improve the image quality. For instance, the number of lines to be regenerated for GRAPPA can be reduced. A reduced data for reduction factor of 4 can be acquired and areduced data for reduction factor 4, can be obtained from it using GRAPPA. SENSE can then be used for reconstruction.

REFERENCES

[1] A. Sodickson, "Breaking the magnetic resonance speed barrier: Implications of parallel imaging," www.appliedradiology.com, Accessed: April, 2005.

[2] B. Madore and N. Pelc, "SMASH and SENSE:Experimental and numerical comparisons," *Magnetic Resonance in Medicine*, vol. 45, pp. 1103–1111, June 2001.

[3] D. Guilfoyle, P. Gibbs, R. Ordidge and P. Mansfield, "Real-time flow measurements using echo planer imaging," *Magnetic Resonance in Medicine*, vol. 18, pp. 1–8. March 1991.

[4] D. Sodickson and W. Manning, "Simultaneous acquisition of spatial harmonics (SMASH):Fast imaging with radiofrequency coil arrays," *Magnetic Resonance in Medicine*, vol. 38, pp. 591–603, July 1997.

[5] D. Walsh, A. Gmitro and M. Marcellin, "Adaptive reconstruction of phased array imagery," *Magnetic Resonance in Medicine*, vol. 43,pp. 683–690, November 2000.

[6] FH. Lin, K. Kwong, J. Belliveau and L. Wald , "Parallel imaging reconstruction using automatic regularization," *Magnetic Resonance in Medicine*, vol. 51, pp. 559–567, March 2004.

[7] J. Henning, A. Nauerth and H. Friedberg, "RARE imaging: A fast imaging method for clinical MRI," *Magnetic Resonance in Medicine*, vol. 3, pp. 832–833, December 1986.

[8] J. Wang, " Using the reference lines to improve the SNR in mSENSE," 10^{th} *Proc. International Society for Magnetic Resonance in Medicine*, Honolulu, HI, USA, May 2002.

[9] K. Pruesmann, M. Weiger, M. Scheidegger and P. Boesiger, "SENSE: Sensitivity encoding for fast MRI," *Magnetoc Resonance in Medicine*, vol. 42, pp. 952–962, November 1999.

[10] K. Scheffler and S. Lehnhardt, "Principles and applications of balanced SSFP techniques," *European Radiology*, vol. 13, pp. 2409–2418, August 2003.

[11] M. Blaimer, F. Breuer, M. Nittka, R. Heidemann, Griswold M., et al., "SMASH, SENSE, PILS, GRAPPA: How to choose the optimal method," *Topics in Magnetic Resonance Imaging*, vol. 15, pp. 223–236, August 2004.

[12] M. Griswold, P. Jakob, M. Nittka, J. Goldfarb and A. Haase, "Partially parallel imaging with localized sensitivities (PILS)," *Magnetic Resonance in Medicine*, vol. 47, pp. 602–609, October 2000.

[13] M. Griswold, P. Jakob, R. Heidemann, M. Nittka, V. Jellus, et al., "Generalized auto-calibrating partially parallel acquisitions (GRAPPA)," *Magnetic Resonance in Medicine*, vol. 47, pp. 1202–1210, June 2002.

[14] P. Jakob, M. Grisowld, R. Edelmann and D. Sodickson, "AUTO-SMASH: A self-calibrating technique for SMASH imaging," *Magnetic Resonance Materials in Physics, Biology and Medicine*, vol. 7, pp. 42–54, November 1998.

[15] P. Lauterber and Z. Liang, *Principles of Magnetic Resonance Imaging: A Signal Processing Perspective*, New York: IEEE Press Series in Biomedical Engineering, 2001, chap. 9, pp. 291–311.

[16] R. Heidemann, M. Griswold, A. Haase and P. Jakob, "VD-AUTO-SMASH imaging", *Magnetic Resonance in Medicine*,vol. 45, pp. 1066–1074,
December 2001.

[17] R. Rzedizan and I. Pykett, "Instant images of human heart using a new whole-body MR imaging system," *American Journal of Roentgenology*, vol. 149, pp. 245–250, 1987.

[18] S. Rane and J. Ji, " A MATLAB toolbox for parallel imaging using multiple phased-array coils," 13^{th} *Proc. International Society for Magnetic Resonance in Medicine*, Miami, FL, USA, May 2004.

[19] S. Wright, M. McDougall and D. Brown, "Single echo acquisition of MR images using RF coil arrays," *Proc. of the Joint EMBS/DEMS Conference*, Houston, TX, USA, October 23-26, 2002.

[20] W. Kyriakos, L. Panych, D. Kacher, CF. Westin, S. Bao, et al., "Sensitivity profiles from an array of coils for encoding and reconstruction in parallel." *Magnetic Resonance in Medicine*, vol. 44,pp. 301–308, February 2000.

[21] Z. Liang, "Improved algorithms for image reconstruction from sensitivity-encoded data ," in *Proc. of the Second Joint EMBS/BMES Conference*, Houston, TX, USA, October 23-26, 2002.

VITA

Swati Dnyandeo Rane received the B.E. degree in electronics and telecommunication from the Pune University, India in 2003. She completed her M.S. in electrical engineering from Texas A&M University, Texas in 2005. Currently, she is pursing the Ph.D. degree in biomedical engineering at Georgia Institute of Technology, Atlanta.

Address for correspondence:
Swati D. Rane
Department of Electrical Engineering
Texas A&M University
214 Zachry Engineering Center
TAMU 3128
College Station, TX 77843

The typist for this thesis was Swati Dnyandeo Rane.